JOURNAL OF MATERIALS SCIENCE 22 (1987) 1135–1140

Mechanical properties of pressure-sintered Al_2O_3–ZrC composites

T. ZAMBETAKIS, J. L. GUILLE, B. WILLER, M. DAIRE
Département Science des Matériaux ENSCS, 1 rue Blaise Pascal, 67008 Strasbourg, France

Alumina–zirconium carbide composites containing up to 0.90 molecular fraction of carbide were prepared by pressure-sintering at 1800 K under pressures of 35 and 50 MPa. Both toughness (evaluated from the indentation cracks length) and flexural strength, first increase with carbide molecular fraction, then decrease. The influence of the sintering pressure is more marked for the toughness than for the flexural strength. The initial increase of the mechanical properties seems to be related to the alumina grain size diminution, and the subsequent decrease to the presence of poorly bonded zirconium carbide agglomerates.

1. Introduction

Introducing a second-phase dispersion in a brittle matrix results in a modification of its mechanical properties. In particular it can produce a substantial improvement of the toughness [1–5] which is most often accompanied by a loss in strength [1, 3–5]. For a given matrix the importance of the modifications depends on the intrinsic properties of the dispersed phase (mechanical behaviour, thermal expansion, phase transformation) and on the dispersion itself (volume fraction, particle form, size and spacing). The present investigation concerns alumina–zirconium carbide composites. Although the literature data concerning zirconium carbide exhibit a wide scatter, the mechanical properties of these two compounds can be regarded as similar and their thermal expansion coefficient as well ($x = 9 \times 10^{-6} K^{-1}$). The main difference lies in their melting points and, as they are related, in their sintering abilities.

2. Experimental procedure and results

2.1. Sample preparation

The composites were fabricated from Alcoa A 16 SG alumina and Cerac "pure" zirconium carbide (99%). The average grain size of the alumina powders is less than 1 μm. The zirconium carbide powder consists of 10 μm average particle size agglomerates, the particle being constituted of several grain (Fig. 1).

The two powders were dry mixed in a mortar for 40 min and then in a planetary ball mill for 30 min more. The mixtures were then uniaxially hot-pressed in graphite dies under an argon atmosphere. The temperature was raised from 20 to 1530° C in 65 min, then kept constant for 30 min (Fig. 2). The carbide molecular fraction was varied from 0 to 0.9 and two series of samples were prepared under 35 and 50 MPa, respectively. The samples obtained were discs, 20 mm in diameter and 10 mm thick. Linear shrinkage is plotted against time in Fig. 2 for some samples. The density was measured by the Archimedes immersion technique and the porosity calculated as a percentage of the theoretical density. The results are listed in Table I. Fig. 3 shows a plot of density and porosity against carbide molecular fraction. It can be seen that the actual density is very close to the theoretical one for carbide molecular fraction up to 0.4, and that the influence of the pressure becomes appreciable for molecular fractions above 0.6. An X-ray diffraction investigation did not show the presence of any other phase than those of the starting materials.

2.2. Mechanical properties

In order to characterize the mechanical properties of the composites two tests were performed: the indentation test and the three-point bend test.

2.2.1. Indentation test

Before testing, all specimens were ground and polished, finishing with 1 μm diamond paste. Tests were performed under 40 N load, using a Vickers indenter mounted on a Frank hardness tester. The K_{IC} values were calculated from the modified Evans and Charles relationship given by Lankford [6]:

$$\left(\frac{K_{IC}\Phi}{Ha^{1/2}}\right)\left(\frac{H}{E}\right)^{0.4} = 0.142(c/a)^{-1.56} \quad (1)$$

where K_{IC}, Φ, H, E, a and c are respectively fracture

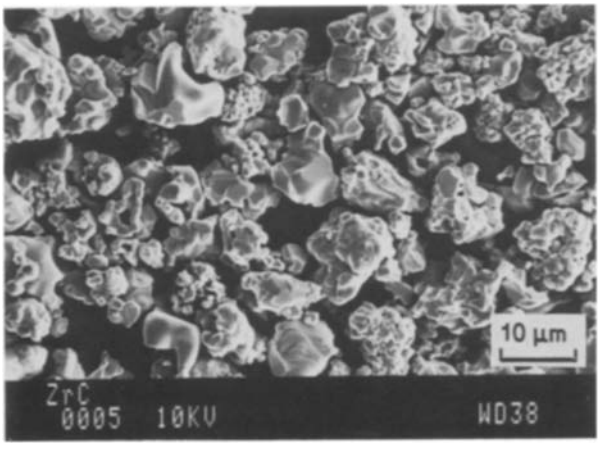

Figure 1 Morphology of the ZrC powder (SEM).

0022–2461/87 $03.00 + .12

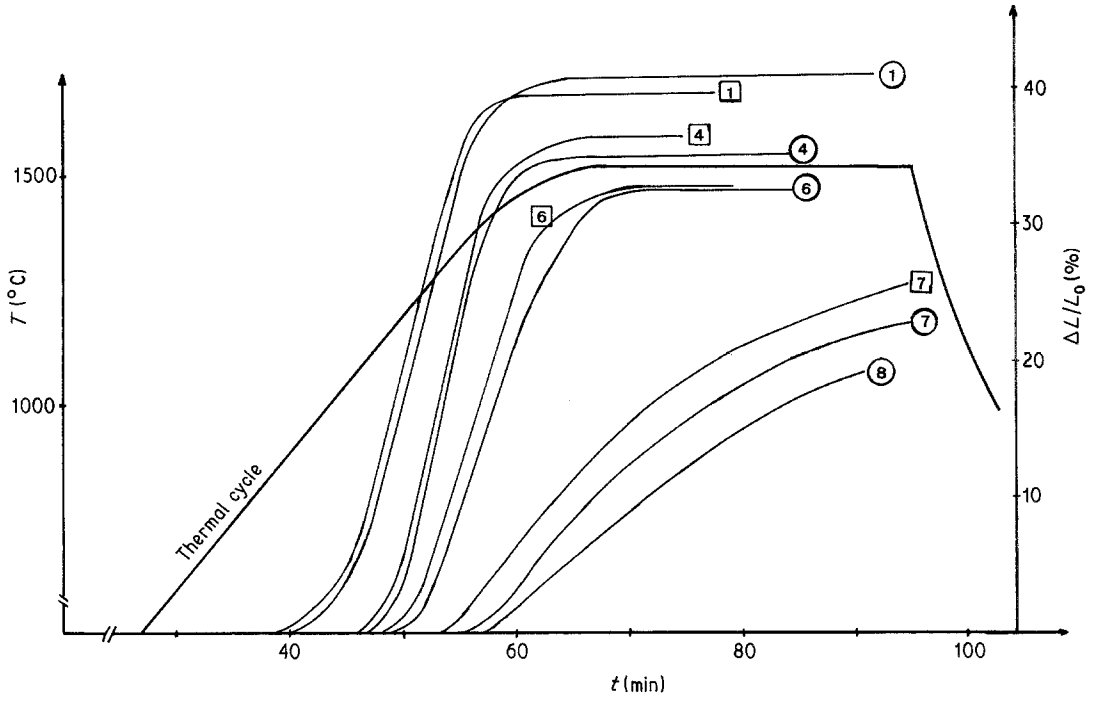

Figure 2 Thermal cycle and linear shrinkage. The numbers refer to Table I. (○) Series I samples (35 MPa), (□) Series II (50 MPa).

toughness, constraint factor ($\simeq 3$), hardness, Young's modulus, half-length of the impression diagonals and indentation crack length. An evaluation of the H/E ratio was obtained from the measurement of the elastic recovery of a Knoop impression, using the semi-empirical formula proposed by Marshall *et al.* [7]:

$$\frac{b'}{a'} \simeq \frac{b'}{a} = \frac{b}{a} - 0.45\frac{H}{E} \qquad (2)$$

where a and b are the diagonal dimensions of the contact area defined by the indenter geometry ($b/a = 7.11$) and a and b the diagonal dimensions of the impression. In order to test the validity of the method two samples were indented under various loads. A plot of ln C against ln P (Fig. 4) shows two straight lines whose slopes are very close to the 0.66 value predicted by Equation 1 if a is expressed as a function of H and P. It proves that the measured K_{IC} values are load-independent. The results of the indentation tests are summarized in Figs. 5 and 6. Plotted against carbide molecular fraction, the Vickers hardness varies little up to 0.6, afterwards it decreases. This is more accentuated for low-pressure samples (Series I). K_{IC} first increases then decreases. The amplitude and the position of the maximum depend markedly on the applied pressure. The low-pressure samples values are always higher.

TABLE I Samples prepared: composition, theoretical density (d_{th}), measured density (d), porosity (p) as a percentage of the theoretical density

Sample	Al_2O_3 (mol %)	ZrC (mol %)	d_{th}	Series I (35 MPa)		Series II (50 MPa)	
				d	p	d	p
Al_2O_3	100		3.981	3.98	0	3.98	0
1	95	5	4.065	4.07	0	4.07	0
2	90	10	4.154	4.14	0.3	4.15	0.1
3	80	20	4.344	4.32	0.6	4.34	0.1
4	70	30	4.551	4.52	0.7	4.53	0.6
5	60	40	4.778	4.72	1.2	4.74	0.9
6	40	60	5.307	5.14	3.1	5.18	2.5
7	80	20	5.963	5.35	10.28	5.48	7.8
8	90	10	6.355	5.10	18.2	5.64	11.2
ZrC		100	6.80		Not sintered		

2.2.2. Three-point bend test

The tests were performed on bars 18 mm × 5 mm × 4 mm. All faces were polished with 7 μm diamond paste. The bars were tested over a 12 mm span at a crosshead speed of 0.2 mm min^{-1}. Flexural strength is plotted against carbide molecular fraction in Fig. 7. It sharply increases for low molecular fraction and then decreases. The differences between low- and high-pressure samples are small, the former being stronger.

3. Discussion

3.1. Fracture toughness

The main mechanisms which may account for the toughness enhancement of a brittle matrix due to a dispersed second phase are all linked to the interaction of the crack front with the dispersed particles. Mostly involved are

(a) energy absorbtion by the second phase, e.g. by plastic deformation;

(b) increase of the fracture surface area caused by surface roughness; and

(c) interaction with the preexisting microcracks.

In the case considered here, the first item cannot play an important role since zirconium carbide does not deform plastically and, although no data were available, there is no reason to suppose that its fracture energy is much higher than that of alumina. The two other items involve the development of residual stresses around the particles as a result of differential contraction. As seen above, there is neither appreciable

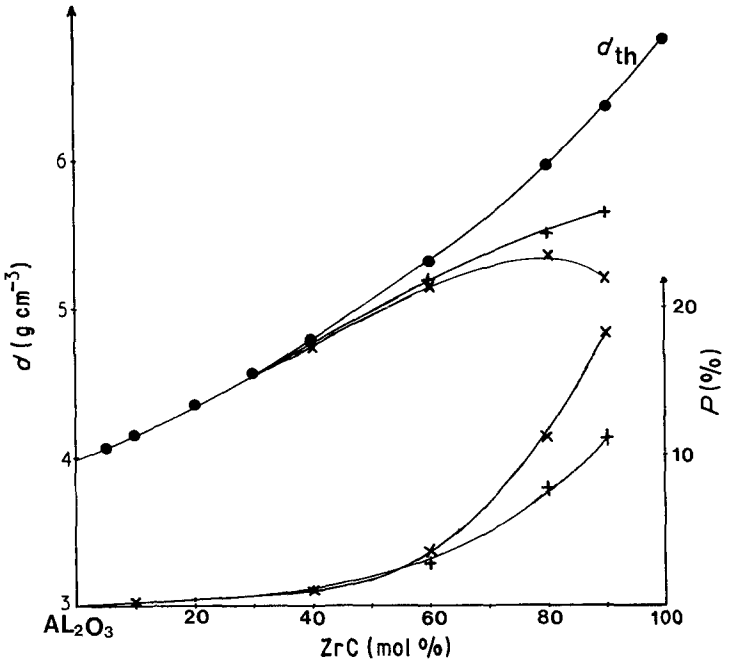

Figure 3 Evolution of the density and the porosity against carbide molecular fraction. d_{th}: theoretical density. (x) Series I, (+) Series II.

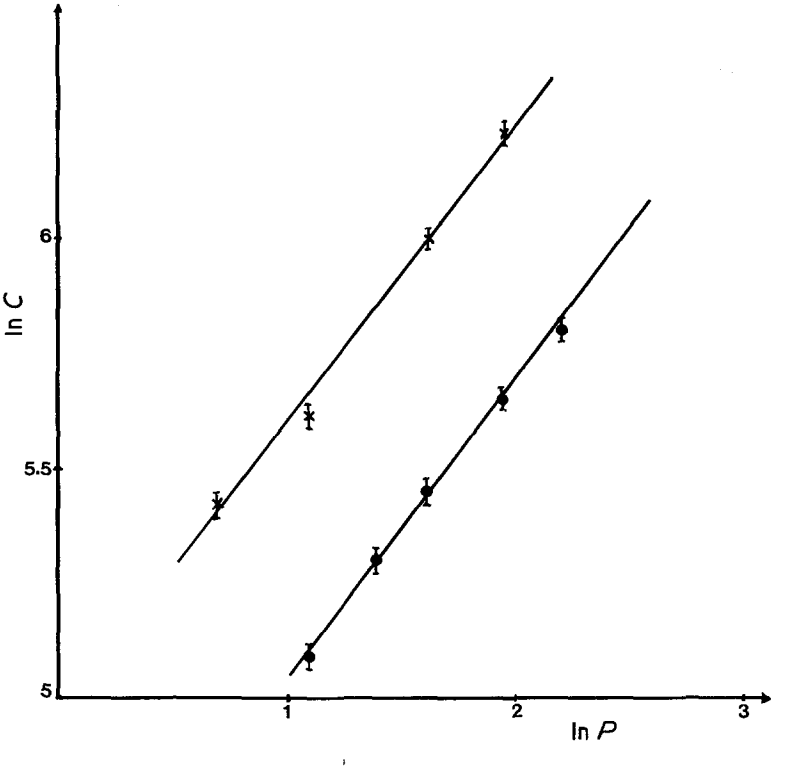

Figure 4 Evolution of the crack length against indentation load for two samples from Series II: (●) Sample 1, (x) Sample 6.

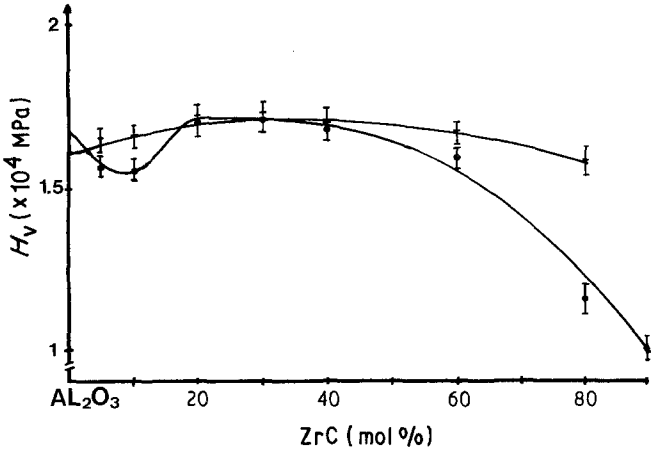

Figure 5 Vickers hardness as a function of the carbide molecular fraction. (●) Series I, (+) Series II.

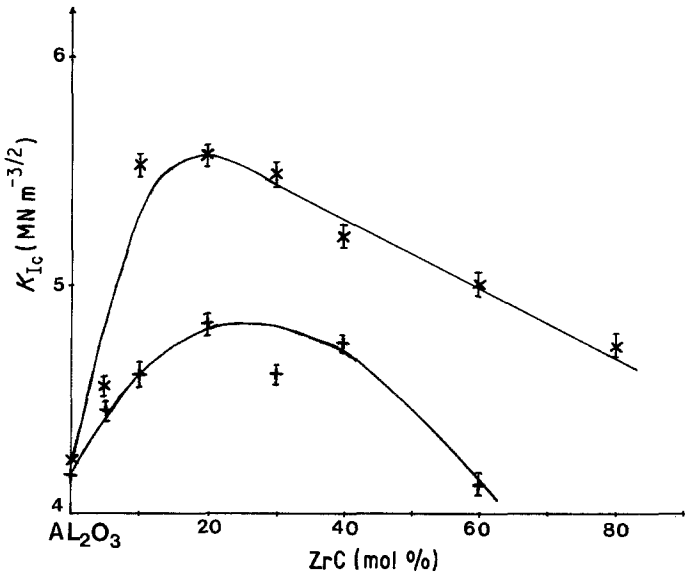

Figure 6 Fracture toughness as a function of the carbide molecular fraction (x) Series I, (+) Series II.

difference in the thermal expansion coefficients nor phase transformation. Furthermore, no direct influence of the carbide grains on the indentation crack paths can be observed (Fig. 8). Thus it may be reasonably thought that none of the above-mentioned mechanisms can account for the observed fracture toughness increase. The SEM examination of fractured samples suggests a different explanation (Fig. 9).

It can be noted that first, the increase of the carbide molecular fraction causes the average grain size to decrease, and second, as the grain size decreases, the mode of rupture tends to evolve from partially transgranular to fully intergranular. The evolution of the toughness may consequently result from two antagonistic phenomena. It first increases because of the decreasing grain size, then decreases when the rupture becomes more intergranular, this being more pronounced as the amount of weak carbide–carbide grain boundaries (and later of the pores) grows. Concerning the marked influence of the pressure a fully convincing explanation was not found. It might be admitted, according to the work of Spriggs *et al.* [8], that a pressure increase retards the intergranular diffusion, causing the grains to be weaker bonded, thus lowering the fracture energy.

3.2. Flexural strength

According to Griffith's theory [9] the tensile strength of a brittle material is given by

$$\sigma = A(\Gamma E/C)^{1/2}$$

where Γ, E and C, are respectively the surface energy, Young's modulus and size of the crack from which catastrophic failure initiates, A being a dimensionless number depending on the mode of loading, the geometry and location of the crack. Since for a fully dense body C is limited to the grain size, lowering it causes C to diminish and, as seen above, Γ (which is related to K_{IC}) to increase. The initial sharp increase of σ with carbide molecular fraction is thus fully comprehensible. The following decrease may result from both lowering the fracture energy and increasing the critical crack size, due to it being no more controlled by the alumina grain size but by one of the poorly bonded carbide agglomerates which become larger with increasing carbide content. Just as in the case of the toughness the influence of the pressure on the strength is not well understood. For a given carbide content no

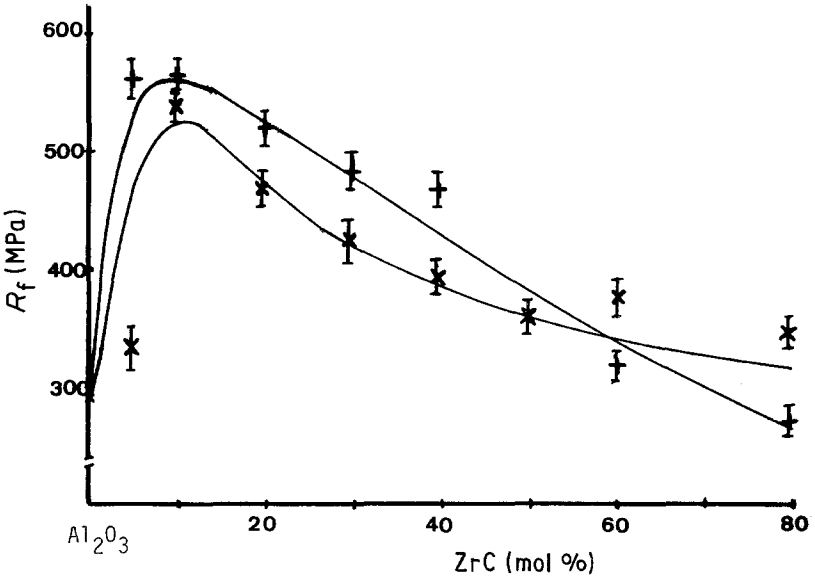

Figure 7 Flexural strength as a function of the carbide molecular fraction (x) Series I, (+) Series II.

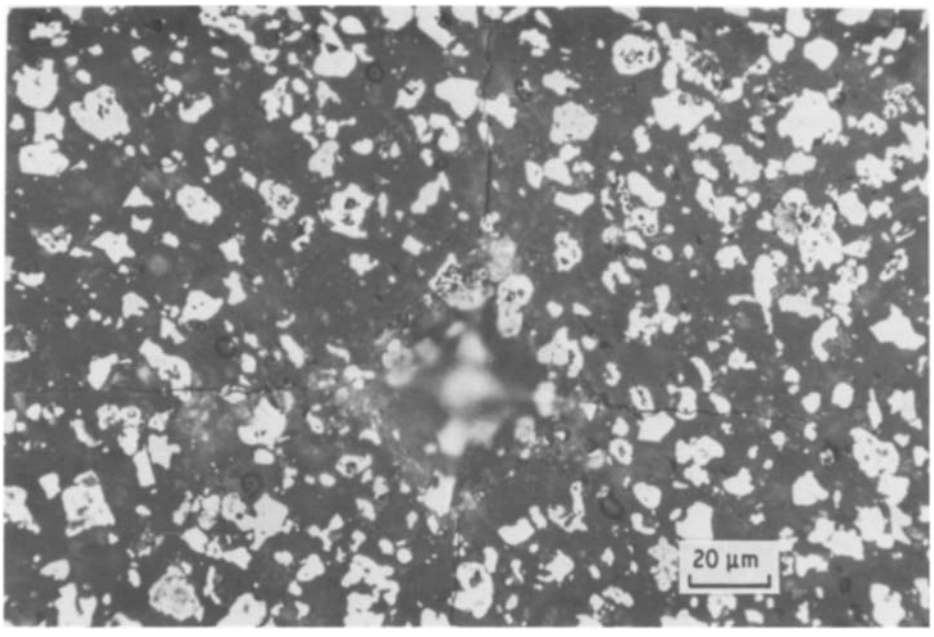

Figure 8 Indentation cracks (× 500).

appreciable difference in grain size was observed between the two series. The relative position of the two curves seems to indicate that the strength depends more on the crack size, the influence of the fracture energy being more pronounced for high carbide contents.

4. Conclusion

For low zirconium carbide molecular fraction, the fabricated composites exhibit a better toughness and strength than pure alumina. This enhancement of the mechanical properties results much more from the modified structure of the matrix than from the presence of the dispersed phase itself. High carbide contents cause the mechanical properties to fall due to the poor sintering ability of the carbide.

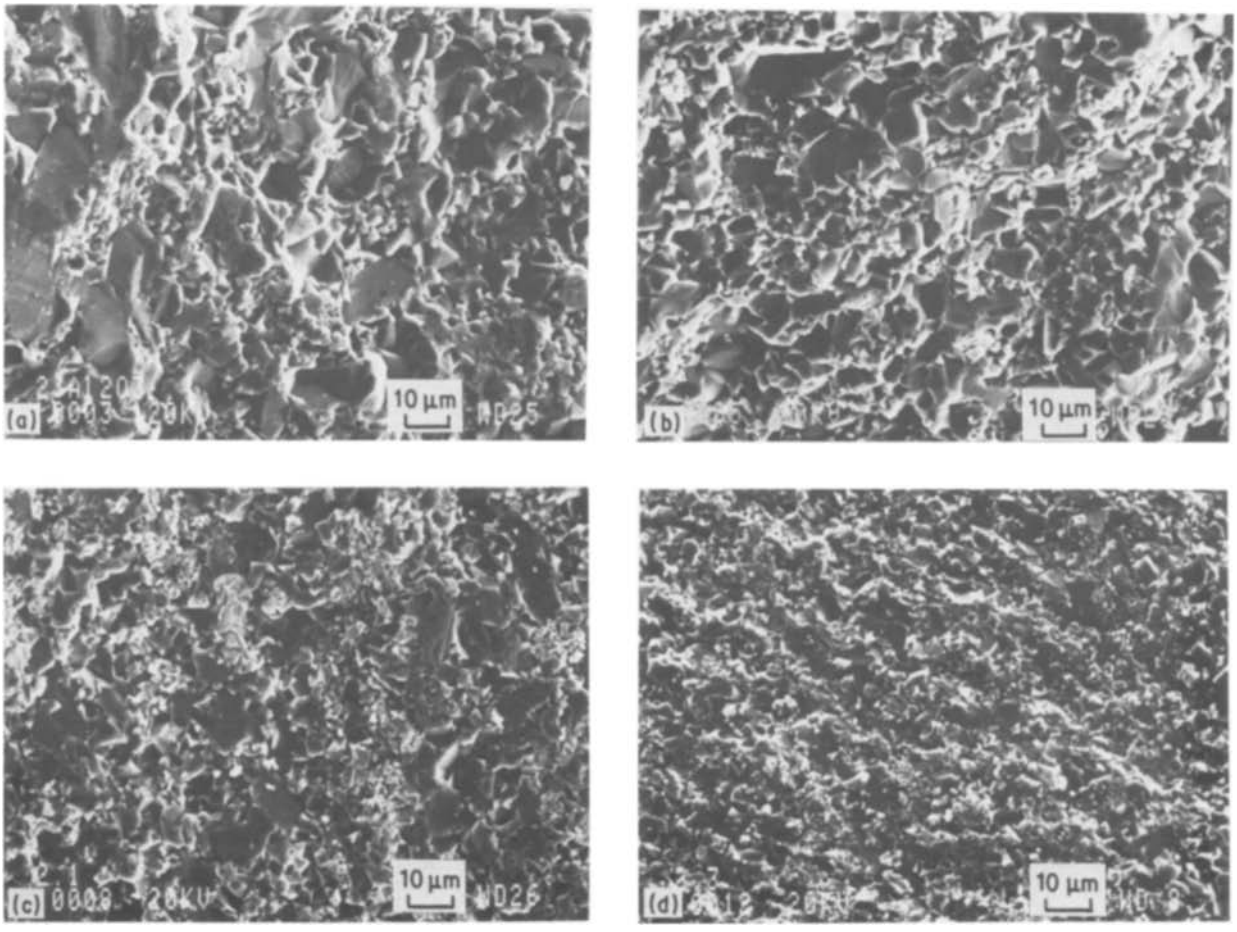

Figure 9 SEM micrographs of the flexion rupture surface. (a) pure alumina, (b) 5% ZrC, (c) 20% ZrC, (d) 40% ZrC.

References

1. F. F. LANGE, *J. Amer. Ceram. Soc.* **54** (1971) 614.
2. P. HING and G. W. GROVES, *J. Mater. Sci.* **7** (1972) 427.
3. F. F. LANGE, *J. Amer. Ceram. Soc.* **56** (1973) 445.
4. N. CLAUSSEN, *ibid.* **59** (1976) 49.
5. T. NOMA and A. SAWAOKA, *J. Mater. Sci.* **19** (1984) 2319.
6. J. LANKFORD, *J. Mater. Sci. Lett.* **1** (1982) 493.
7. D. B. MARSHALL, T. NOMA and A. G. EVANS, *J. Amer. Ceram. Soc.* **65** (1982) C175.
8. R. M. SRRIGS, L. A. BRISSETTE and T. VASILOS, *Amer. Ceram. Soc. Bull.* **43** (1964) 572.
9. A. A. GRIFFITH, *Phil. Trans. Soc.* **A221** (1920) 163.

Received 9 June
and accepted 30 June 1986